Supplementary Figures

a

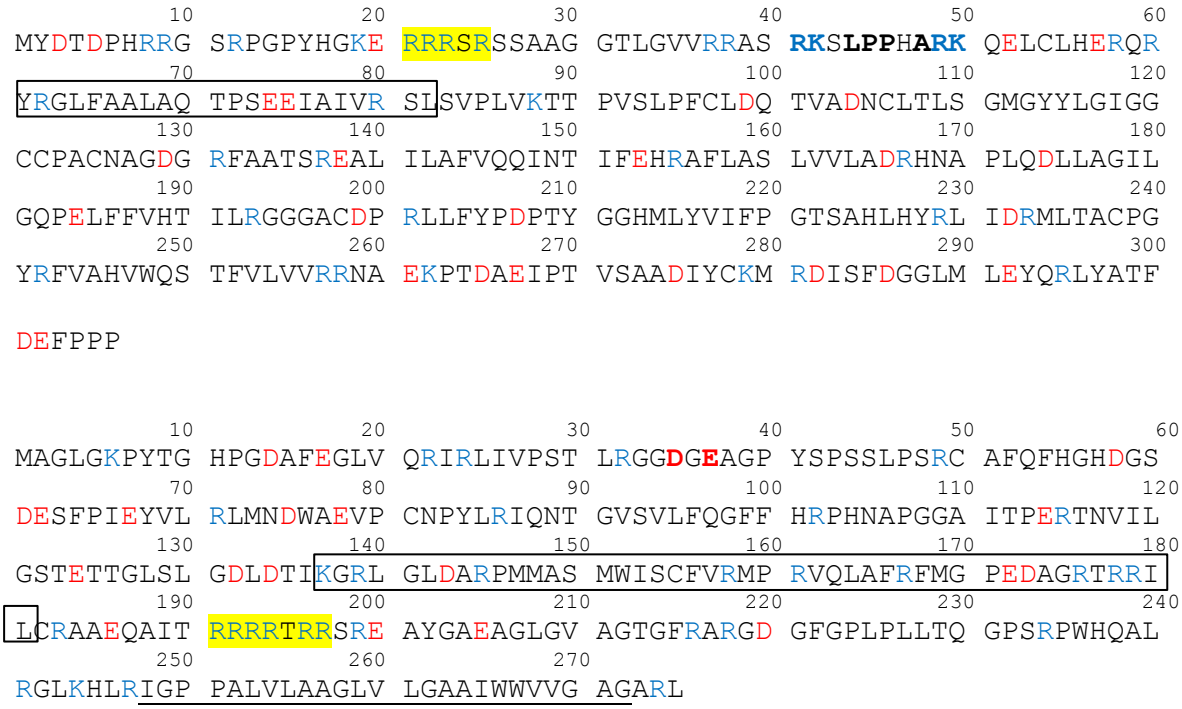

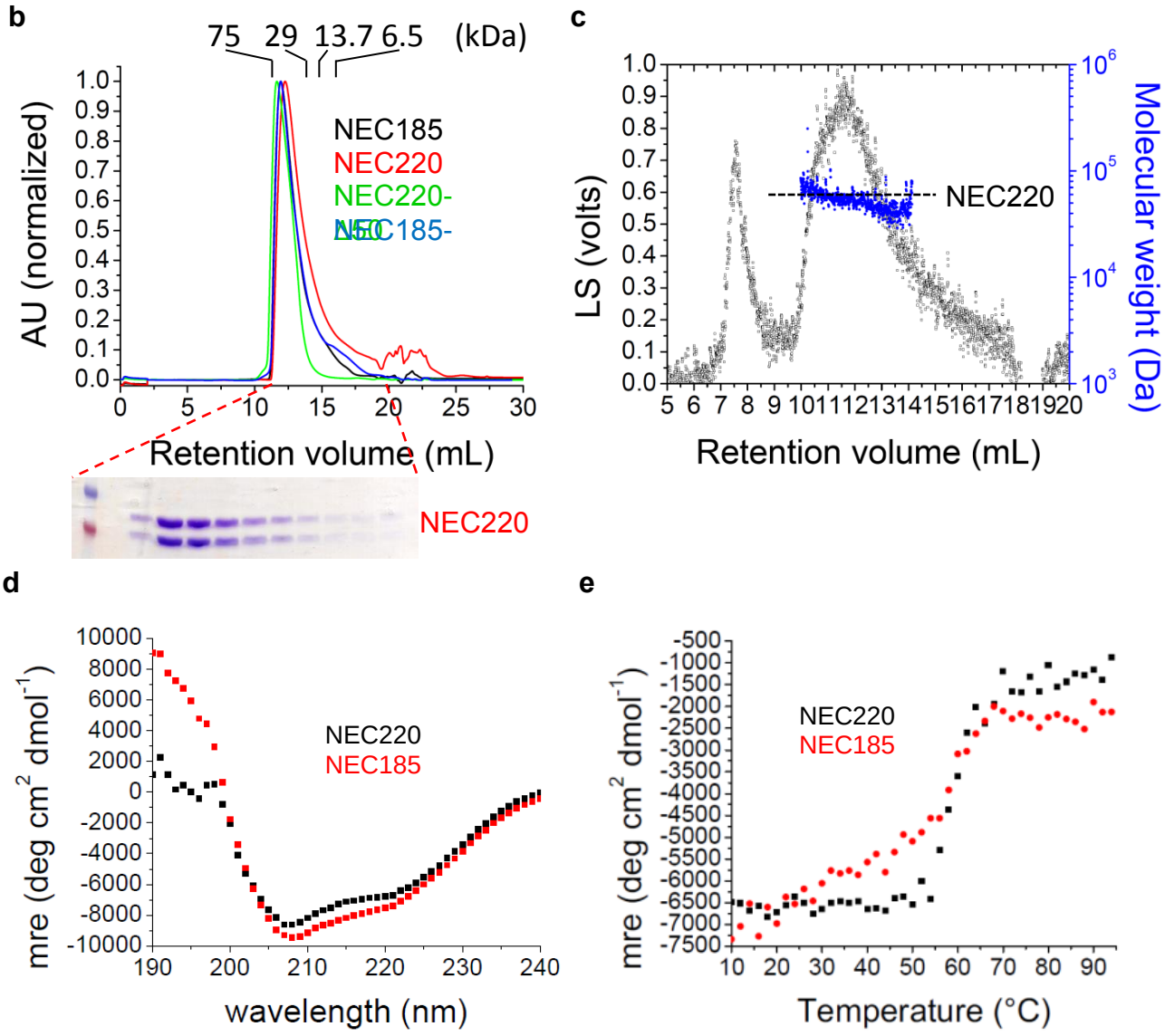

Supplementary Figure 1. Recombinant soluble NEC is a stable, properly folded heterodimer. a, Sequences of HSV-1 strain F UL31 (top) and UL34 (bottom). The transmembrane region in UL34 is underlined and the nuclear localization sequences are highlighted in yellow. The predicted respective binding sites for UL31 and UL34 are boxed and sites of mutations used in this study are in bold. Charged residues are shown in standard colors. **b**, Overlay of size-exclusion chromatograms of NEC220, NEC220-Δ50, NEC185, and NEC185-Δ50. The elution volumes of the molecular weight standards are marked above the chromatogram. All four complexes are heterodimers judging by their elution volumes on the

size-exclusion chromatography. As an example, a Coomassie stained SDS-PAGE gel is shown below, which corresponds to the depicted gel filtration trace of NEC220. **c**, SEC-coupled multi-angle light scattering (MALS) analysis of NEC220. The experimentally determined molecular weight is 58.92 kDa, which corresponds to a heterodimer of UL31 and UL34. The signal from the 90°-scattering detector (black) is plotted against the left Y-axis. Average molecular weights are plotted in blue against the right Y-axis. The theoretical molecular weight for a heterodimer (59.39 kDa) is shown as a horizontal dashed black line. **d-e**, NEC220 and NEC185 are properly folded as determined using circular dichroism (CD) spectroscopy. The secondary structure content of 20% α-helix and 24% β-strand calculated from the CD spectra (**d**) is consistent with secondary structure predictions using Jpred 3 [1]. **e**, Thermal denaturation stability of NEC220 and NEC185 as monitored by measuring change in the CD signal at 222 nm with increasing temperature. The complexes are stable with melting temperatures of 58.3±0.5 °C for NEC220 and 58.5±0.5 °C for NEC185, respectively. Data are shown as mean residual ellipticity (mre) vs. temperature.

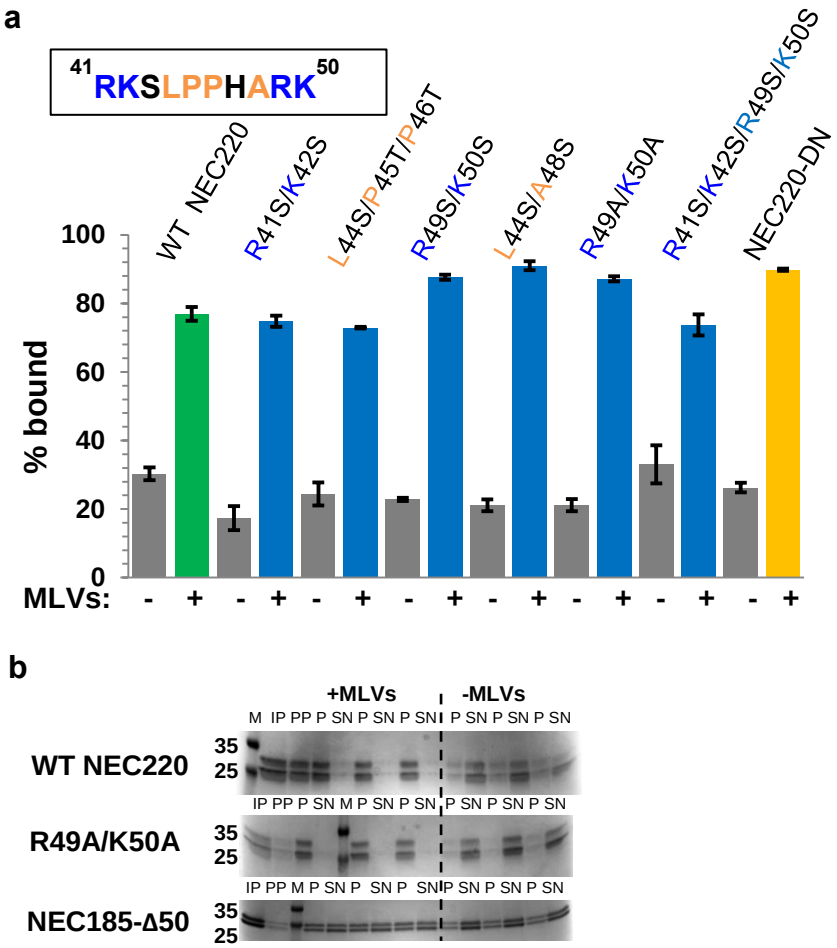

Supplementary Figure 2. Membrane interaction is not impaired by mutagenesis of residues 41-50 of UL31. Membrane binding of the WT and mutant NEC220 was quantified using a pelleting assay with PC/PS/PA MLVs. All protein samples were centrifuged prior to adding the liposomes to account for nonspecific protein aggregation. For negative controls, all proteins were also pelleted in the absence of liposomes. Error bars represent the standard error of measurement of three individual experiments. **a,** Point mutations within the N terminus of UL31 do not affect membrane binding. NEC220-DN binds as well as NEC220. **b**, Representative gels from pelleting assay used for quantification (M = standard, IP = input, PP = protein pellet, P = pelleted fraction, SN = supernatant).

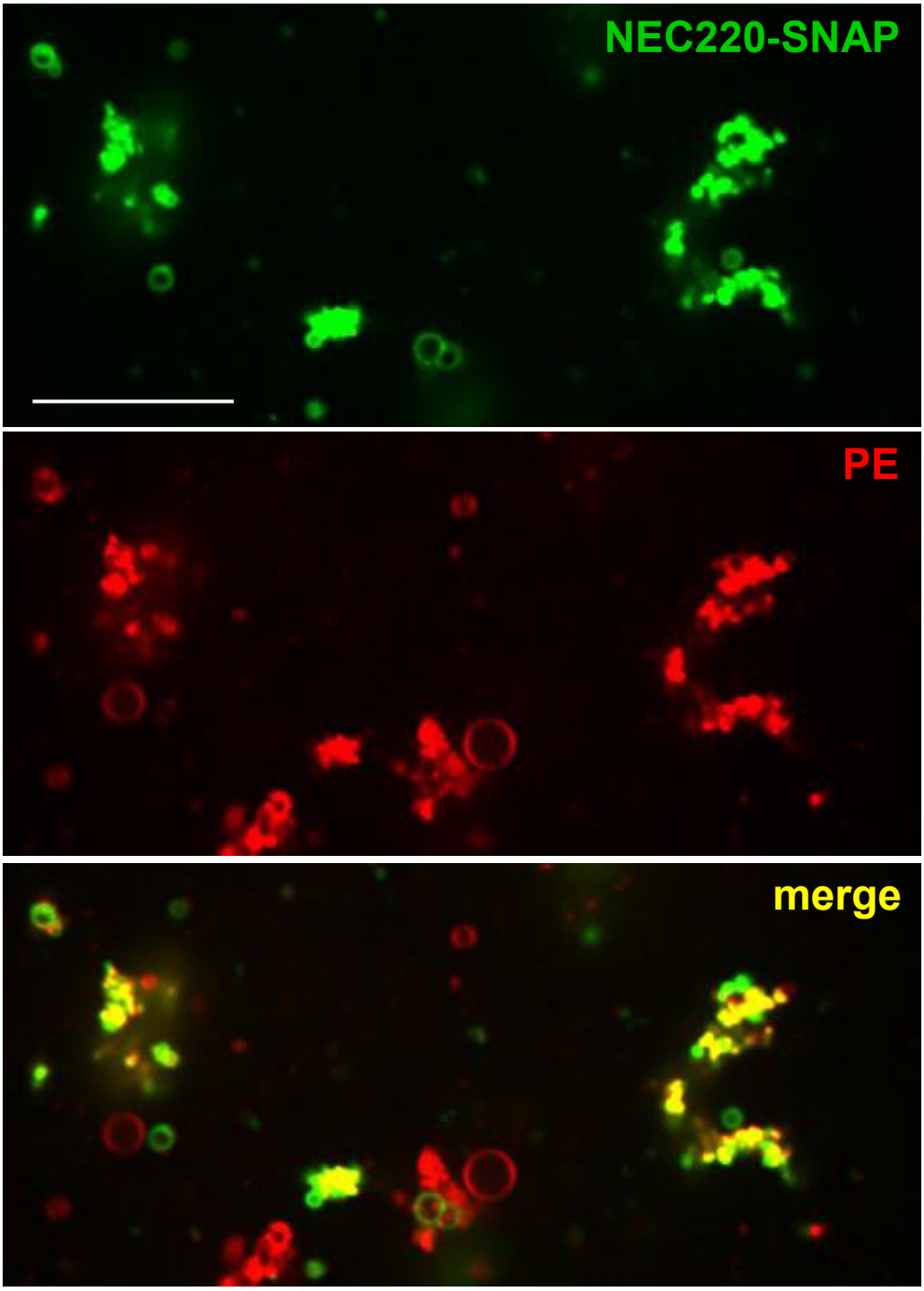

Supplementary Figure 3. Long incubation times of GUVs with NEC220 or incubation in the presence of high amounts of NEC220 produce aggregates containing protein and membranes. The scale bar represents 15 µm.

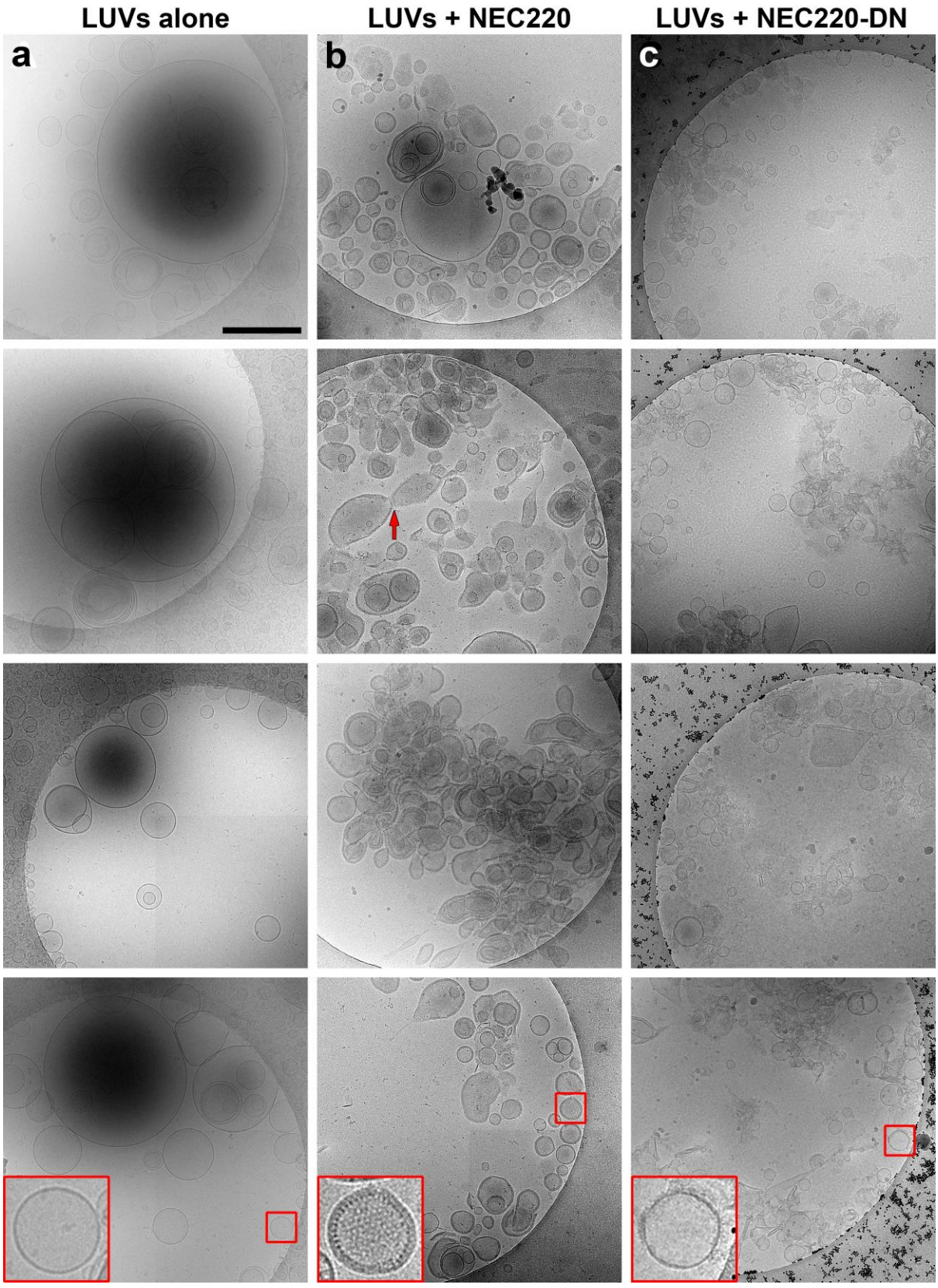

Supplementary Figure 4. Additional 2D cryo-EM images of LUVs. a, LUVs alone. **b,** LUVs with NEC220. Arrow points at two linked vesicles, presumably connected by the

NECs bound to the outer surfaces (a rare occurrence). The protein “fence” linking these vesicles is longer than a single NEC, and each “fence post” in it is probably formed by two NEC molecules that are bound to the outer surface of the two vesicles and interact using their membrane-distal regions. In such an arrangement, the forces driving negative curvature would cancel each other out leading to flat surfaces that cannot bud in either direction. **c**, LUVs with NEC220-DN. Scale bar is 500 nm, and all images are on the same scale. Red squares in the bottom row show close-ups of similar sized LUVs alone, LUVs with NEC220 and LUVs with NEC220-DN mutant. Note that the NEC220 forms a highly regular "fence posts" arrangement on the inside of LUVs while the mutated NEC220-DN shows less regular attachment to the outside of LUVs.

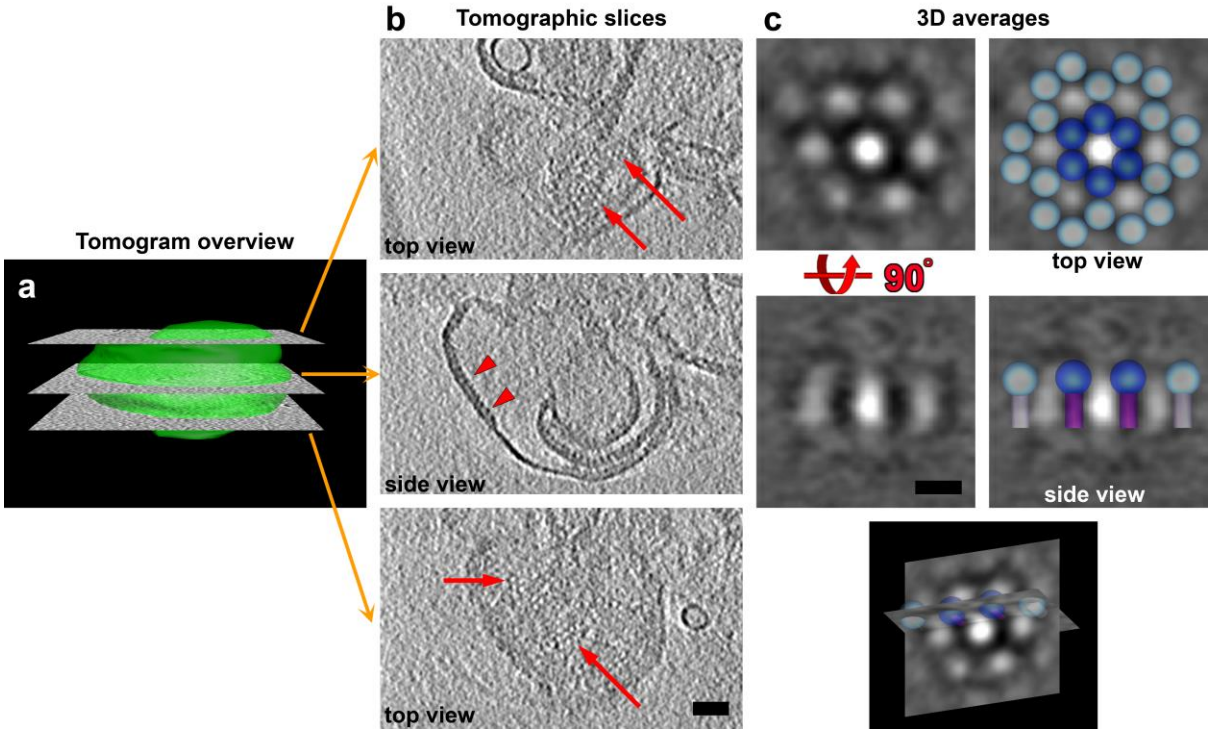

Supplementary Figure 5. 3D insights into LUVs with NEC220. a, Tomogram overview highlighting a LUV (green) and the position of the three tomographic slices shown in panel. **b**, Three tomographic slices showing the NEC220 hexamers as rings (marked with arrows) in top view (top and bottom end of LUV) and as longitudinal "fences" (marked with arrow heads) in side view in the middle of the LUV. Scale bar is 50 nm. **c**, 3D averages and the schematic model of the NEC220 hexagonal array. 240 NEC220 hexamers were averaged with imposed 6-fold symmetry and clearly show that rings visible in top views and fences visible in side views are the same structure viewed from two different orientations. Scale bar is 10 nm.

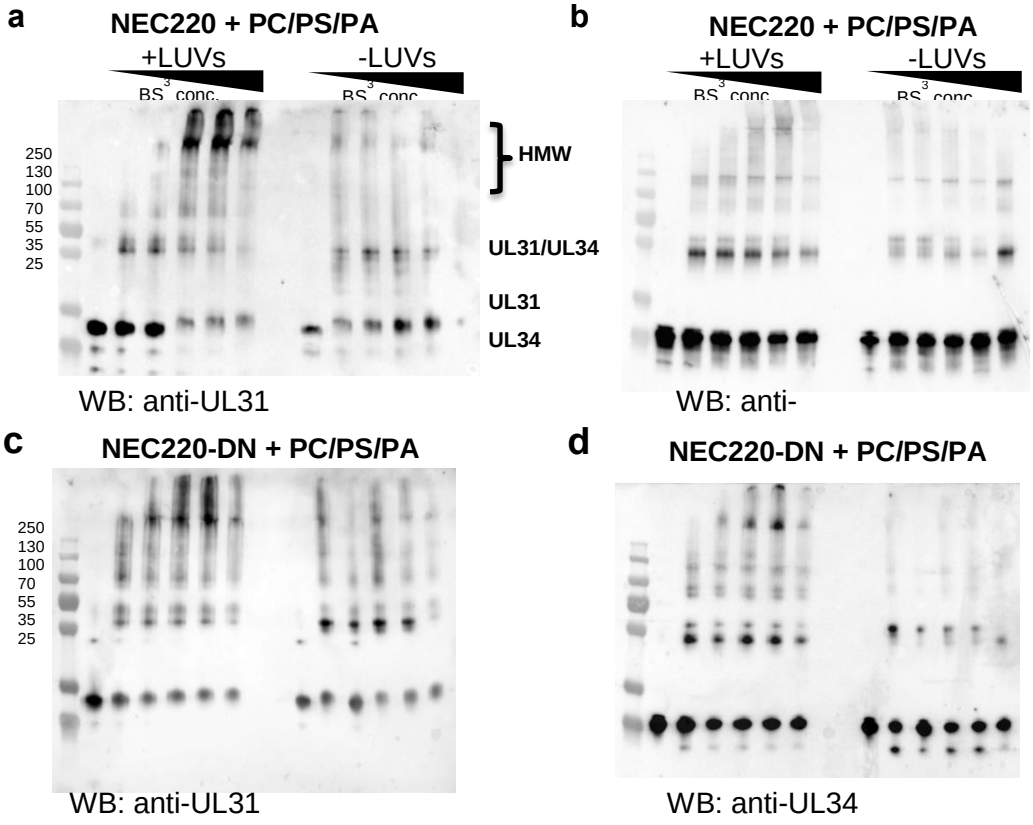

Supplementary Figure 6. High-molecular-weight species of crosslinked NEC220 contain more UL31 than UL34. a-d, BS^3 was added at 0, 25, 50, 250, 500, 2500-fold molar excess. Samples were analyzed by 12% SDS-PAGE and Western blot.

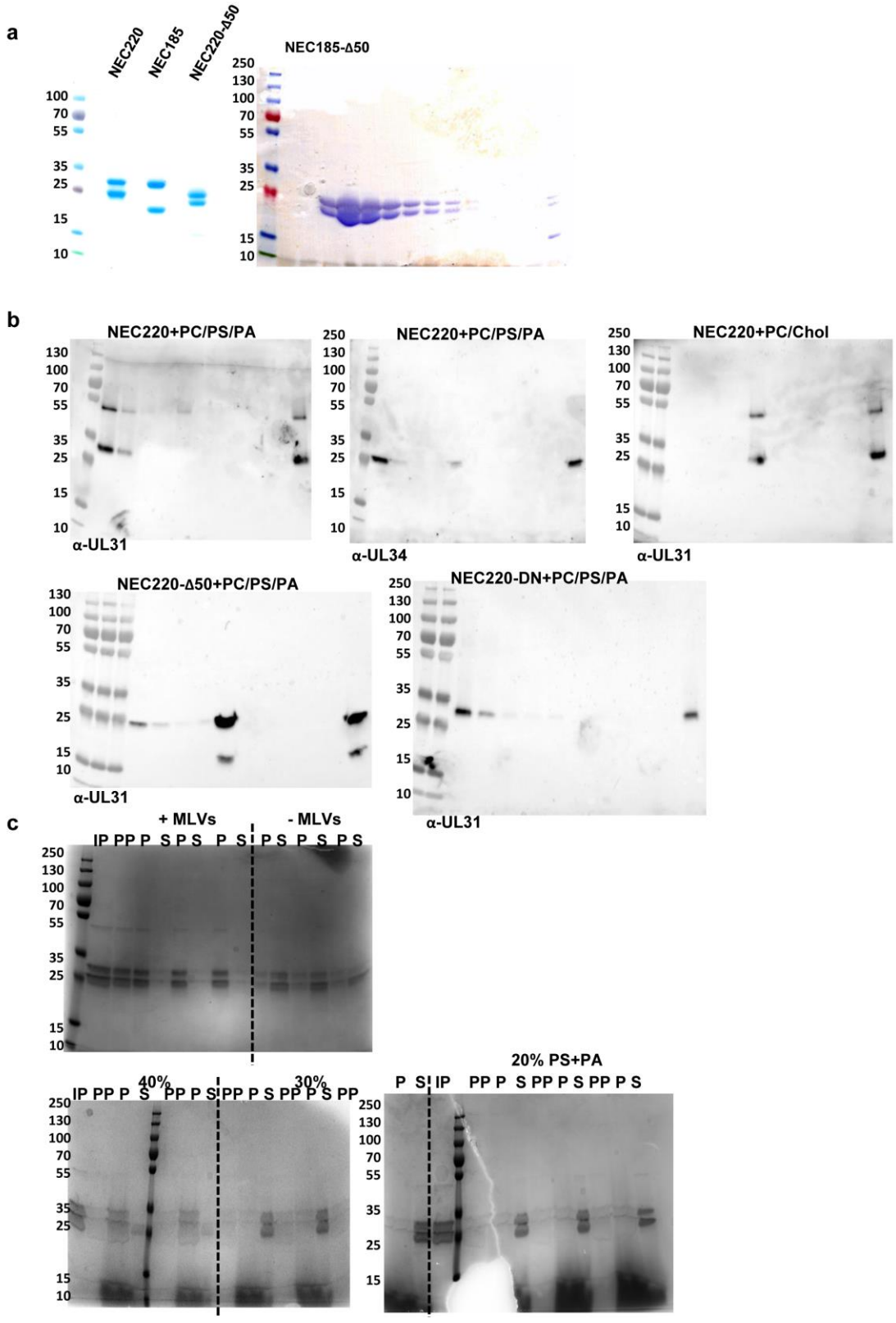

Supplementary Figure 7. Original SDS gels and western blots shown in figures 1b and 2a-b.

Supplementary References

1. Cole, C., Barber, J.D. & Barton, G.J. The Jpred 3 secondary structure prediction server. *Nucleic Acids Res* **36**, W197-201 (2008).